Membrane Biology:

Modeling, Substrate Docking, and Mutational Analysis Identify Residues Essential for the Function and Specificity of a Eukaryotic Purine-Cytosine NCS1 Transporter

Emilia Krypotou, Vasiliki Kosti, Sotiris Amillis, Vassilios Myrianthopoulos, Emmanuel Mikros and George Diallinas

J. Biol. Chem. 2012, 287:36792-36803.
doi: 10.1074/jbc.M112.400382 originally published online September 11, 2012

THE JOURNAL OF BIOLOGICAL CHEMISTRY VOL. 287, NO. 44, pp. 36792–36803, October 26, 2012

Modeling, Substrate Docking, and Mutational Analysis Identify Residues Essential for the Function and Specificity of a Eukaryotic Purine-Cytosine NCS1 Transporter*[S]

Received for publication, July 12, 2012, and in revised form, September 7, 2012 Published, JBC Papers in Press, September 11, 2012, DOI 10.1074/jbc.M112.400382

Emilia Krypotou[‡1], Vasiliki Kosti[‡1], Sotiris Amillis[‡], Vassilios Myrianthopoulos[§], Emmanuel Mikros[§], and George Diallinas[‡2]

From the [‡]Faculty of Biology, University of Athens, Panepistimiopolis, Athens 15784, Greece and [§]School of Pharmacy, University of Athens, Panepistimiopolis, Athens 15771, Greece

Background: The purine-cytosine FcyB transporter is a prototype member of the NCS1 family.
Results: Using homology modeling, substrate docking, and rational mutational analysis, we identify residues critical for function and specificity.
Conclusion: Important aspects concerning the molecular mechanism and evolution of transporter specificity are revealed.
Significance: The first systematic approach on structure-function-specificity relationships in a eukaryotic NCS1 member is shown.

The recent elucidation of crystal structures of a bacterial member of the NCS1 family, the Mhp1 benzyl-hydantoin permease from *Microbacterium liquefaciens*, allowed us to construct and validate a three-dimensional model of the *Aspergillus nidulans* purine-cytosine/H^+ FcyB symporter. The model consists of 12 transmembrane α-helical, segments (TMSs) and cytoplasmic N- and C-tails. A distinct core of 10 TMSs is made of two intertwined inverted repeats (TMS1–5 and TMS6–10) that are followed by two additional TMSs. TMS1, TMS3, TMS6, and TMS8 form an open cavity that is predicted to host the substrate binding site. Based on primary sequence alignment, three-dimensional topology, and substrate docking, we identified five residues as potentially essential for substrate binding in FcyB; Ser-85 (TMS1), Trp-159, Asn-163 (TMS3), Trp-259 (TMS6), and Asn-354 (TMS8). To validate the role of these and other putatively critical residues, we performed a systematic functional analysis of relevant mutants. We show that the proposed substrate binding residues, plus Asn-350, Asn-351, and Pro-353 are irreplaceable for FcyB function. Among these residues, Ser-85, Asn-163, Asn-350, Asn-351, and Asn-354 are critical for determining the substrate binding affinity and/or the specificity of FcyB. Our results suggest that Ser-85, Asn-163, and Asn-354 directly interact with substrates, Trp-159 and Trp-259 stabilize binding through π-π stacking interactions, and Pro-353 affects the local architecture of substrate binding site, whereas Asn-350 and Asn-351 probably affect substrate binding indirectly. Our work is the first systematic approach to address structure-function-specificity relationships in a eukaryotic member of NCS1 family by combining genetic and computational approaches.

Purines and pyrimidines (nucleobases) are absolutely essential metabolites for all cells, being not only the precursors of nucleotide and nucleic acid biosynthesis but also being involved in cell signaling, nutrition, response to stress, and cell homeostasis. Most cells in all domains of life possess specific nucleobase transporters, distinct from those involved in the uptake of nucleosides (1, 2). Nucleobase transporters are important in protozoan and plant development and in the susceptibility of human, protozoan, or fungal cells to purine-related drugs (3–10). Fungi possess three evolutionary distinct families of transporters specific for nucleobases (2, 11, 12). Members of one of them, the so called nucleobase cation symport (NCS1,[3] also known as purine-related transporter) family, are ubiquitously distributed in all fungi and are present in some eubacteria, archaea (11–14), and plants (15) but are absent in protozoa and metazoa (see uniprot online). Besides purines, cytosine, and uracil, other known substrates for NCS1 transporters include the antifungals 5-fluorocytosine (5-FC), and 5-fluorouracil, benzyl-hydantoin, allantoin, thiamine, pyridoxal-based compounds, and nicotinamide riboside. All NCS1 members of known function probably act as H^+ symporters, although the *Microbacterium liquefaciens* benzyl-hydantoin transporter was reported to be a Na^+ symporter (11).

The NCS1 family includes two major subfamilies, the Fcy-like and the Fur-like transporters (11). Three Fcy-like proteins of Ascomycetes have been well characterized genetically and studied with respect to regulation of expression, transport kinetics, and substrate specificity. These are the Fcy2p (16), Fcy21p (17), and FcyB (13) permeases of *Saccharomyces cerevi-*

* This work was supported in part by the John S. Latsis Public Benefit Foundation.
[S] This article contains supplemental Tables S1 and S2 and Figs. 1–3.
[1] Co-financed by the European Union (European Social Fund) and Greek national funds through the Operational Program "Education and Lifelong Learning" of the National Strategic Reference Framework-Research Funding Program: THALIS and Heracleitus II, Investing in knowledge society through the European Social Fund.
[2] To whom correspondence should be addressed. Tel.: 30(210)7274649; Fax: 30(210)7274702; E-mail: diallina@biol.uoa.gr.

[3] The abbreviations used are: NCS1, nucleobase cation symport 1; TMS, transmembrane segment; 5-FC, 5-fluorocytosine; IFD, induced fit docking; MM, minimal media; ER, endoplasmic reticulum; mRFP, monomeric red fluorescent protein.

siae, *Candida albicans*, and *Aspergillus nidulans*, respectively. All three are involved in high affinity transport of adenine, hypoxanthine, guanine, cytosine, and 5-FC. The only physiological difference between Fcy2p/Fcy21p and FcyB is that the two yeast transporters constitute the sole high capacity gateways for purine uptake, whereas in *A. nidulans* high capacity purine uptake is catalyzed by another transporter, called AzgA (17), FcyB acting basically as a cytosine supplier and only secondarily as a purine carrier (13).

Despite some classical genetic approaches in Fcy2p that identified several residues critical for substrate or cation binding and transport (18–20), very little was known with respect to structure-function relationships in NCS1-like transporters until recently. In 2008, however, the crystal structure of a bacterial member of the NCS1 family, namely the Mhp1 benzyl-hydantoin permease from *M. liquefaciens* (21), was reported (22). Surprisingly, the Mhp1 topology has proved to be very similar to that of several recently revealed structures of other bacterial transporters that showed no sequence similarity and exhibited entirely different specificities. These include the amino acid transporter LeuT (23), the galactose transporter vSGLT (24), the betaine transporter BetP (25), and two amino acid transporters, AdiC (26) and ApcT (27). Dysfunction of members of this growing superfamily in humans is associated with neurological (28) and kidney disorders (29), cancer (30), and drug resistance (31). The core of the fold shared by these transporters is an "inverted repeat" motif with two sets of five transmembrane helices oppositely orientated with respect to the membrane (often called the 5HIR-fold) (32–34). The two extra TMSs (TMS11 and TMS12 in the NCS1 family) do not seem to participate in transport activity, and their role is unclear.

Most interestingly, several different conformations have been observed for these transporters in the recent years. These can be categorized into three classes: outward-facing, as observed in LeuT (35, 36), Mhp1 (22), and AdiC (26, 37); occluded, where a trapped substrate is blocked from exiting on either side of the protein as seen in LeuT (23), Mhp1 (22), BetP (25), and AdiC (37); inward-facing, as seen in Mhp1 (34), vSGLT (24), ApcT (27), and LeuT (36). Up to date, Mhp1 and LeuT are the only transporters trapped into three structural conformations associated with transport catalysis. From analyses of these three structures and molecular dynamics simulations, a mechanism has been proposed for the transport cycle in Mhp1 or LeuT (34, 36, 38). Switching from the outward- to the inward-facing state goes through occluded states and is primarily achieved by a rigid body movement of several TMSs (*e.g.* 3, 4, 8, and 9 in Mhp1) relative to a rather rigid bundle of helices (1, 2, 6, and 7 in Mhp1). In the occluded transient states, "thin gates" involving only a few residues in specific TMSs (*e.g.* 5 and 10 in Mhp1) and parts of loops control the opening and closing of the substrate binding site to the exterior or interior. This forms the basis of an alternating access mechanism applicable to probably all transporters of the 5HIR superfamily (32–34, 36, 39). Evidently, details of substrate transport, especially those concerning the occlusion mechanism, remain largely controversial because models have been derived by comparing transporters with divergent amino acid sequences that transport a wide variety of substrates and that possibly select and transport different ions (Na^+ *versus* H^+) for driving the symport of their major substrates (34, 36, 38). Furthermore, what is often ignored is that all available structures concern prokaryotic transporters, which despite being similar to important mammalian carriers, also present significant structural and biochemical differences. For example, eukaryotic transporters possess long N- and C-tails or longer hydrophilic loops, absent in prokaryotes, that are often associated with transporter subcellular trafficking, function, specificity, stability, or topology (40–42).

In this work we construct and validate a three-dimensional model of the *A. nidulans* purine-cytosine FcyB transporter based on the outward facing substrate-occluded crystal structure of the Mhp1 benzyl-hydantoin permease from *M. liquefaciens* (PDB entry 2JLO). Subsequently, we use this model to perform independent docking studies and thus identify residues that might be involved in substrate binding and transport. Most importantly, we experimentally validate our speculations on specific amino acid residues by a systematic functional analysis of relevant mutants. Our work is discussed with respect to the molecular determinants underlying substrate specificity in the NCS1 family.

EXPERIMENTAL PROCEDURES

Homology Modeling—Proteins with significantly similar structural-fold with FcyB were identified using HHpred. All 5HIR transporters showed significant similarity with FcyB, but only Mhp1 showed a 100% probability (*E* value $1.8E^{-55}$; *p* value $6.6\ E^{-60}$). Homology model building was performed using MODELLER v.9.8 software (43).

Protein Preparation—The protein was prepared for docking calculations using the Protein Preparation Workflow (Schrödinger Suite 2011 Protein Preparation Wizard) implemented in the Schrödinger suite and accessible from within the Maestro program (Maestro, Version 9.2, Schrödinger, LLC, NY, 2011). Briefly, hydrogen atoms were added, and the orientation of hydroxyl groups, Asn, Gln, and the protonation state of His were optimized to maximize hydrogen bonding. Finally, the ligand-protein complex was refined with a restrained minimization performed by Impref utility that is based on the Impact molecular mechanics engine (Impact Version 5.7, Schrödinger, LLC, NY, 2011) and the OPLS2001 force field, setting a max root mean square deviation of 0.30 (44). Ligand preparation for docking was performed with LigPrep (LigPrep, Version 2.5, Schrödinger, LLC, NY, 2011) application that consists of a series of steps that perform conversions, apply corrections to the structure, generate ionization states and tautomers, and optimize the geometries.

Molecular Dynamic Simulations—For the molecular dynamics simulations, Desmond v.3 software was implemented (Desmond Molecular Dynamics System, Version 3.0, D. E. Shaw Research, NY). The system was prepared by embedding the protein in a 1-palmitoyl-2-oleylphosphatidylcholine (POPC) lipid bilayer, solvating the membrane by TIP4P explicit water, neutralizing with counter ions, and adding 150 mM salt and subsequently following the stepwise equilibration protocol as developed by Desmond for membrane proteins (45). The ori-

entation of the protein in the bilayer was determined by using the Mhp1 template available in OPM database (46). An 18-ns simulation was performed in the NPγT ensemble with Langevin thermostat and barostat and semi-isotropic pressure restraints (supplemental Fig. S1).

Induced Fit Docking—Molecular docking was performed using the induced fit docking (IFD) protocol (Schrödinger Suite 2011 Induced Fit Docking protocol) that is intended to circumvent the inflexible binding site and accounts for the side chain or backbone movements or both upon ligand binding (47). In the first stage of the IFD protocol, softened-potential docking step, 20 poses per ligand were retained. In the second step for each docking pose, a full cycle of protein refinement was performed with Prime 1.6 (Prime, Version 3.0, Schrödinger, LLC, NY, 2011) on all residues having at least one atom within 8.0 Å of an atom in any of the 20 ligand poses. The Prime refinement starts with a conformational search and minimization of the side chains of the selected residues, and after convergence to a low energy solution, an additional minimization of all selected residues (side chain and backbone) is performed with the truncated-Newton algorithm using the OPLS parameter set and a surface Generalized Born implicit solvent model. The obtained complexes are ranked according to Prime calculated energy (molecular mechanics and solvation), and those within 30 kcal/mol of the minimum energy structure are used in the last step of the process, redocking with Glide 5.7 (Glide, Version 5.7, Schrödinger, LLC, NY, 2011) using standard precision and scoring. In the final round, the ligands used in the first docking step are redocked into each of the receptor structures retained from the refinement step. The final ranking of the complexes is done by a composite score that accounts for the receptor-ligand interaction energy (GlideScore) and receptor strain and solvation energies (Prime energy).

Media, Strains, Growth Conditions, and Transformation Genetics—Standard complete and minimal media (MM) for *A. nidulans* were used. Media and supplemented auxotrophies were at the concentrations given online in fgsc. Nitrogen sources were used at the final concentrations, 5 mM urea, 10 mM $NaNO_3$, 0.5 mM purines. *Escherichia coli* was grown on Luria-Bertani medium. Media and chemical reagents were obtained from Sigma or AppliChem (Bioline Scientific SA, Hellas, Greece). Transformations were performed as described previously (48). A single-copy plasmid integration of the FcyB served as a standard wild-type control. A Δ*fcyB*::*argB*; Δ*uapA*; Δ*uapC*::*AFpyrG*; Δ*azgA*; *riboB2*; *pabaA1* mutant strain (13) was the recipient strain in transformations with the wild-type pAN520, the pAN530, the pAN540 (see below), or the mutant FcyB alleles carried on the above vectors. As a negative, transformants with empty pAN vectors were used. These vectors allow selection of transformants based on *p*-aminobenzoic acid (*pabaA1*) or riboflavin (*riboB2*) auxotrophy complementation. Transformants expressing intact *fcyB* or *fcyB-gfp* alleles, through either single-copy or multi-copy plasmid integration events, were identified by PCR and Southern analysis. For the relative subcellular localization of wild-type or mutant N81A FcyB-GFP with mRFP-tagged histone H1 (HhoA-mRFP), appropriate strains were constructed by standard genetic crossing. The strain harboring HhoA-mRFP is reported in Edgerton-Morgan and Oakley (49). Growth tests were performed at 25 and at 37 °C, pH 6.8.

Plasmid Constructions and FcyB Mutations—pAN520 is a modified pBluescript KS(+) vector (Stratagene) based on the plasmid pAN510 (50) that carries the FcyB orf cloned in-frame between the 5′ and 3′ regulatory sequences of the *uapA* gene and also carrying the *pabaA* gene as a selection marker (13). pAN530 and pAN540 are similar to pAN520, but in this case the *fcyB* and the *fcyB* fused C- or N-terminally with the *gfp* together with the 5′ and 3′ regulatory sequences of the *uapA* gene were cloned in the pGEM™-T vector (Promega), also carrying the *riboB* gene from *Aspergillus fumigatus* as a selection marker. Mutations were constructed by site-directed mutagenesis according to the instructions accompanying the QuikChange® site-directed mutagenesis kit (Stratagene) on the above vectors and were confirmed by sequencing. Oligonucleotides used for cloning and site-directed mutagenesis purposes are listed in supplemental Table S1.

Standard Nucleic Acid Manipulations—Genomic DNA extraction from *A. nidulans* was as described in fgsc. Plasmid preparation from *E. coli* strains and DNA bands were purified from agarose gels done with the Nucleospin Plasmid kit and the Nucleospin ExtractII kit according to the manufacturer's instructions (Macherey-Nagel, Lab Supplies Scientific SA, Hellas, Greece). Southern blot analysis was performed as described previously (51). [^{32}P]dCTP-labeled molecules used as *fcyB*-, *riboB*-, or *pabaA*-specific probes were prepared using a random hexanucleotide primer kit following the supplier's instructions (Takara Bio, Lab Supplies Scientific SA) and purified on MicroSpin™ S-200 HR columns following the supplier's instructions (Roche Diagnostics). Labeled [^{32}P]dCTP (3000 Ci/mmol) was purchased from the Institute of Isotopes Co. Ltd, Miklós, Hungary. Restriction enzymes were from Takara Bio. Conventional PCR reactions were done with KAPATaq DNA polymerase (Kapa Biosystems, Lab Supplies Scientific SA). Cloning and amplification of products were done with Pfx Platinum (Invitrogen) or Phusion® Flash High-fidelity PCR MasterMix (New England Biolabs, Lab Supplies Scientific SA).

Membrane Protein Extraction and Western Blot Analysis—Cultures for membrane protein extraction were grown in MM supplemented with urea at 37 °C for 8 h. Membrane protein extraction was performed as previously described (52). Equal sample loading was estimated by Bradford assays. Total proteins (30 μg) were separated by SDS-PAGE (10% w/v polyacrylamide gel) and electroblotted (Mini PROTEAN™ Tetra Cell, Bio-Rad) onto PVDF membranes (Macherey-Nagel, Lab Supplies Scientific SA) for immunodetection. The membrane was treated with 3% (w/v) BSA, and immunodetection was performed with a primary mouse anti-GFP monoclonal antibody (Roche Diagnostics) or a mouse anti-actin monoclonal (C4) antibody (MP Biomedicals Europe, Lab Supplies Scientific SA) and a secondary goat antimouse IgG HRP-linked antibody (Cell Signaling Technology Inc., Bioline Scientific SA). Blots were developed by the chemiluminescent method using the LumiSensor Chemiluminescent HRP Substrate kit (Genscript USA, Lab Supplies Scientific SA) and SuperRX Fuji medical X-Ray films (FujiFILM Europe, Lab Supplies Scientific SA).

Kinetic Analysis—[^{3}H]Hypoxanthine (19.6–33.4 Ci/mmol, Moravek Biochemicals, CA) uptake in MM was assayed in germinating conidiophores of *A. nidulans* concentrated at 10^7 conidiospores/100 μl at 37 °C, pH 6.8, as previously described (40, 53). Initial velocities were measured at 1 min of incubation with concentrations of 0.2–2.0 μM [^{3}H]hypoxanthine at the polarity maintenance stage (3–4 h, 130 rpm). $K_{m/i}$ values were obtained directly by performing and analyzing uptakes (Prism 3.02: GraphPad Software) using labeled hypoxanthine at 0.2–0.5 μM or at various concentrations (0.5–2000 μM) of non-labeled substrates. K_i values were calculated by satisfying the criteria for use of the Cheng and Prusoff equation $K_i = IC_{50}/(1 + (L/K_m))$ in which L is the permeant concentration. IC_{50} values were determined from full dose-response curves, and in all cases the Hill coefficient was close to −1, consistent with the presence of one binding site. Reactions were terminated with the addition of equal volumes of ice-cold MM containing 1000-fold excess of non-radiolabeled substrate. Background uptake values were corrected by subtracting either values measured in the deleted mutants or values obtained in the simultaneous presence of 1000-fold excess of non-radiolabeled substrate. Both approaches led to the same background uptake level, not exceeding 10–15% of the total counts obtained in wild-type strains. All transport assays were carried out in at least three independent experiments, with three replicates for each concentration or time point. S.D. was < 20%.

Epifluorescence Microscopy—Samples for fluorescence microscopy were prepared as previously described (52). In brief, germlings incubated on coverslips in liquid MM supplemented with $NaNO_3$ as the nitrogen source for 12–14 h at 25 °C were observed on an Axioplan Zeiss phase-contrast epifluorescent microscope, and the resulting images were acquired with a Zeiss-MRC5 digital camera using the AxioVs40 V4.40.0 software. Image processing, contrast adjustment, and color combining were made using the Adobe Photoshop CS4 Extended Version 11.0.2 software or the ImageJ software. Images were converted to 8-bit grayscale or RGB and annotated using Photoshop CS4 before being saved to TIFF.

RESULTS

FcyB Structural Model—The construction of a structural model of FcyB was based on the crystal structure of the Mhp1 benzyl-hydantoin permease from *M. liquefaciens* (PDB entry 2JLO (22)). The two proteins share a rather moderate sequence similarity (18% identity), which is, however, adequate for sustaining a theoretical model of FcyB. The model built here was based on the alignment of the two proteins, as shown in a multiple alignment including all NSC1 carriers with known function, which was further modified manually (Fig. 1). Model building was performed using MODELLER software. The loop refinement routine and a slow simulated annealing protocol for model refinement were implemented. As a first validation of the model, the structure with the best spatial restraints score was subjected to a 18-ns molecular dynamics run using Desmond software. The system was prepared by embedding the protein in a POPC lipid bilayer and solvating the membrane by explicit water. The root mean square deviation of the transmembrane helices α-carbons from starting coordinates was monitored throughout the simulation and did not exceed 3 Å, thus indicating the stability of the theoretical model.

The overall three-dimensional structure of the FcyB model (Fig. 2) corresponds to an outward-facing conformer made of 12 TMSs that adopt a mostly helical secondary structure. The architecture of the transporter divides it in two distinct domains, a compact core consisting of segments TMS1–10 and a C-terminal domain made of TMS11–12. The transmembrane helices in the core are connected with rather short loops (<14 amino acid residues), whereas the loop separating the core and TMS11–12 is longer (23 residues). The distribution of the ionized residues on the protein surface is reasonable, as most of them are positioned either at the cytoplasmic and periplasmic sides or along the protein pore in the protein interior. Positive charges are mostly concentrated in the cytoplasm-facing loops. The core of FcyB is subdivided in two inverted repeats made of TMS1–5 and TMS6–10, arranged in a 2-fold pseudosymmetry axis, running parallel with the membrane plane. The two repeat units are completely intertwined, giving two topologically distinct subdomains made of TMSs 1, 2, 6, and 7 and TMSs 3, 4, 8, and 9, respectively, linked with helices TMS5 and TMS10. As will be shown below, the substrate binding site is located in the space between the two subdomains of the core (see Fig. 2*B*).

Substrate Docking in FcyB—Using the FcyB model, aspects of substrate recognition were addressed using docking calculations. The four major physiological substrates, namely hypoxanthine, adenine, guanine, and cytosine, as well as the antifungal 5-FC were docked to the modeled structure of FcyB. Calculations were performed using the IFD protocol as introduced by the Schrödinger 2011 Suite of programs. The IFD protocol is based on an iterative implementation of Glide algorithm for rigid docking and Prime algorithm for protein refinement, resulting in an improved simulation of binding in terms of protein flexibility. Furthermore, because Prime is a modeling tool especially developed for refinement of protein structures derived by homology, its implementation as part of the IFD protocol was considered in the case of FcyB as promising. The best orientation for each substrate was finally selected on the basis of lowest energy, number of intermolecular interactions, and visual inspection.

Fig. 3 shows the modeled interactions of FcyB with its four physiological substrates and the antifungal 5-FC. FcyB interacts with adenine through a bidentate H bond that is formed between Asn-163 and ligand sites C6-NH_2 and N1, an H bond between Ser-85 and purine N7, and π-π stacking of the purine ring between the indole rings of Trp-159 and Trp-259 (Fig. 3*A*). FcyB interacts with hypoxanthine and guanine through the establishment of three H bonds between Asn-163 and N1-H, between Ser-85 and C2=O_2, and between Asn-354 and N3, as well as π-π stacking of the purine ring between Trp-159 and Trp-259 (Fig. 3, *B* and *C*). Finally, FcyB interacts with cytosine and its toxic analog 5-FC by forming three H bonds between Asn-163 and N3, between Asn-354 and ligand C4-NH_2, and between Ser-85 and C2=O_2 as well as π-π stacking with Trp-159 and Trp-259 (Fig. 3, *D* and *E*).

These results establish that Asn-163 and the two invariable Trp residues, Trp-159 and Trp-259, interact with similar positions of the rings of all purines and cytosine, whereas the inter-

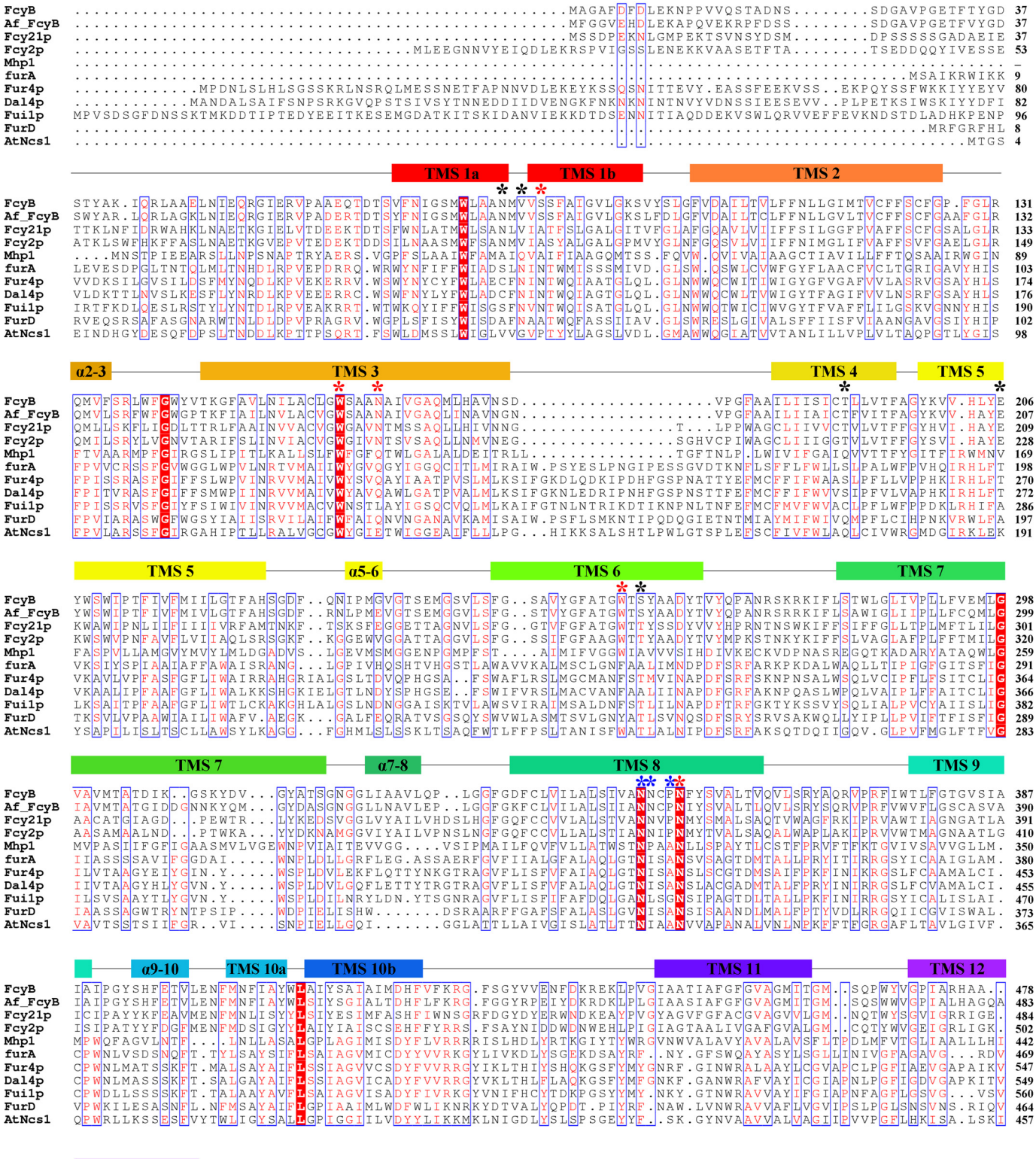

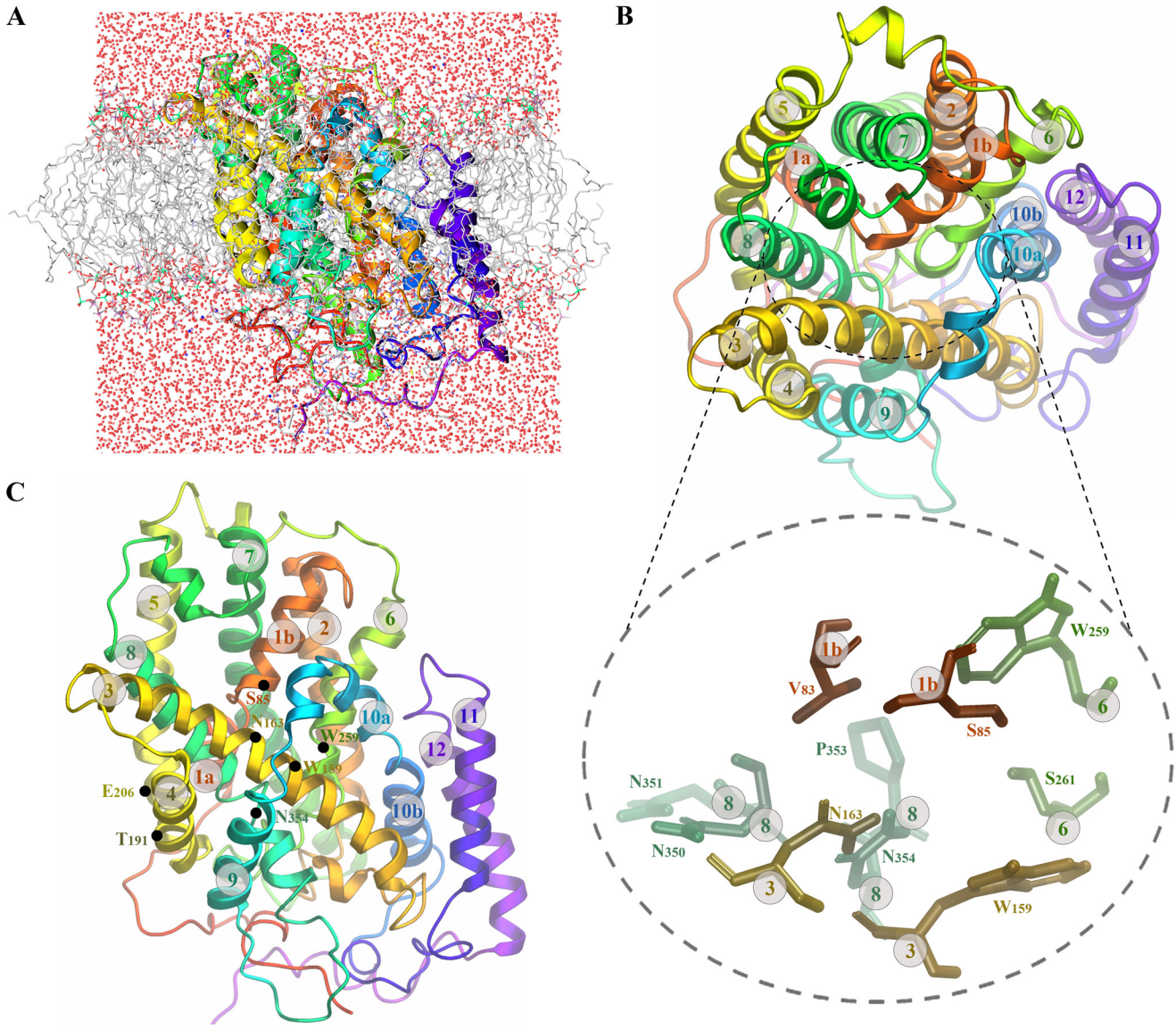

FIGURE 2. **FcyB structural model.** *A*, shown is the modeled three-dimensional structure of FcyB validated with molecular dynamics using Desmond software. *B*, shown is the top view of the FcyB model where the core of the first 10 TMSs is clearly distinguished from the last two TMSs 11 and 12, which probably do not affect transport catalysis *per se*. The core can also be seen as two subdomains, the first made of TMSs 1, 2, 6, and 7 and the second from TMSs 3, 4, 8, and 9, linked with flexible helices TMS5 and TMS10. The substrate binding site is located in the space between the two subdomains of the core. In the *lower panel*, the topology of residues critical for the function of the substrate binding site, Ser-85, Trp-159, Asn-163, Trp-259, Asn-350, Asn-351, Pro-353, and Asn-354, is shown in zoom-out. *C*, shown is the side view of the FcyB structure showing the topology of residues Ser-85, Trp-159, Asn-163, Trp-259, and Asn-354, involved in direct interactions with substrates (see also Fig. 3). Residues Thr-191 and Glu-206 are also shown (see Results). TMS regions are highlighted with colors as in Fig. 1.

actions involving Ser-85 and Asn-354 vary depending on the substrate docked. As will be shown and discussed later, mutational analysis strongly support the docking results. In addition, the model and docking analysis showed that two neighboring Asn residues, Asn-350 and Asn-351, might interact with Asn-354 in a way that probably builds a necessary architecture for substrate binding (see also supplemental Fig. S2). The importance of residues Asn-350 and Asn-351 in substrate binding was rigorously established through mutational analysis in this work (see later). Finally, in the docking models for purine binding, Ser-261 was also within H bond distance from either N3 (adenine) or N9-H (hypoxanthine, guanine). However, in this case, mutational analysis did not support the involvement of Ser-261 in direct substrate binding (see also later).

FIGURE 1. **Multiple sequence alignment of FcyB and NCS1 homologues of known function.** The three-dimensional FcyB model was constructed on the basis of the alignment shown with Mhp1. Putative TMSs of FcyB are denoted in *colored cylinders*. Invariant and highly conserved amino acids are shaded in *red* and *blue-lined boxes*, respectively. Amino acids critical for function and specificity discussed in the Results are highlighted with *asterisks*: *red* for residues interacting with substrates, *blue* for those critical for substrate binding and transport, and *black* for other residues discussed in the Results. The listed NCS1 homologues include: FcyB of *A. nidulans*, GI: 169798762; AfFcyB of *A. fumigatus* (Af_FcyB), GI: 169798764; Fcy21p of *S. cerevisiae*, GI: 392860008; Fcy2p of *S. cerevisiae*, GI: 6320897; Mhp1 of *M. liquefaciens*, GI: 210060746; FurA of *A. nidulans*, GI: 2876438; Fur4p of *S. cerevisiae*, GI: 6319495; Dal4p of *S. cerevisiae*, GI: 392860728; Fui1p of *S. cerevisiae*, GI: 6319429; FurD of *A. nidulans*, GI: 149212441; AtNcs1 of *Arabidopsis thaliana*; GI: 16648836. All Fcy-like proteins are purine-cytosine transporters. Fur4p and FurD are uracil transporters. FurA and Dal4p are allantoin transporters. Fui1p is a uridine transporter. AtNCS1 is reported to be specific for adenine-guanine-uracil transport, but no direct information on its ability to transport other nucleobases exists (15).

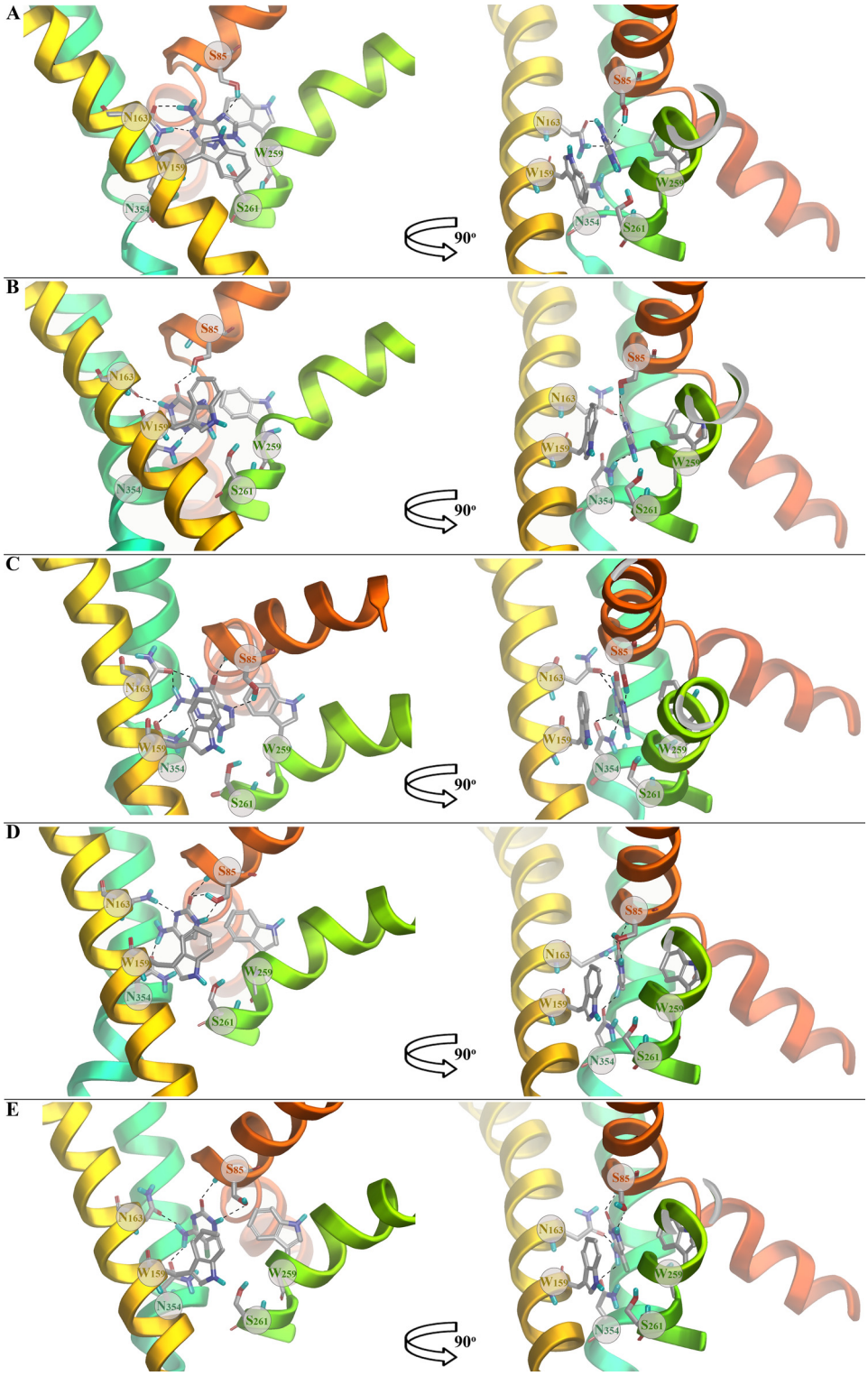

FIGURE 3. **Substrate docking in FcyB.** *A*, adenine. *B*, hypoxanthine. *C*, guanine. *D*, cytosine. *E*, 5-FC. Hydrogen bonds are depicted with *dashed lines*.

Rational Design and Construction of FcyB Mutants—Results derived from docking methodologies suggested that five residues in FcyB might be directly involved in substrate binding. These are Ser-85 in TMS1, Trp-159 and Asn-163 in TMS3, Trp-259 in TMS6, and Asn-354 in TMS8. Two more Asn residues, Asn-350 and Asn-351, might also interact with Asn-354 in a way that is critical for substrate binding. Five of these putatively functional residues, Trp-159, Asn-163, Trp-259, Asn-350, and Asn-354, superimpose with amino acid residues, which have been shown to directly interact with the substrate (benzyl-hydantoin) in Mhp1, namely Trp-117, Gln-121, Trp-220, Asn-314, and Asn-318. Interestingly, these residues are either absolutely (Trp-117, Asn-314, and Asn-318) or highly (Trp-220 and Gln-121) conserved in the NCS1 family (see Fig.

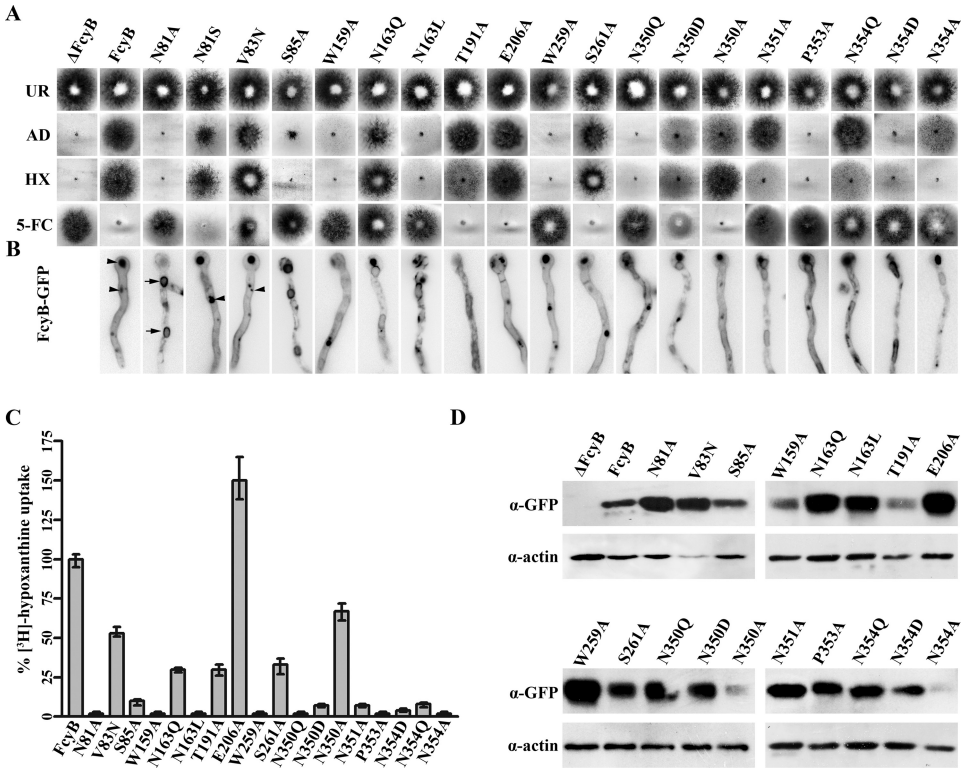

FIGURE 4. **Functional analysis of FcyB mutations.** *A*, shown are growth tests on purines as sole nitrogen sources and resistance/sensitivity test on 5-FC at 25 °C. *AD* is adenine, and *HX* is hypoxanthine. Growth on urea is also shown (*UR*) as a control. Positive (FcyB) and negative (ΔFcyB) isogenic control strains are shown. *B*, epifluorescence microscopy showing *in vivo* subcellular expression of FcyB-GFP mutant alleles and a wild-type control (FcyB) is presented as *dark structures in a grayscale inverted mode*. In selected samples, *arrows* and *arrowheads* depict perinuclear ER membrane rings (verified by DAPI staining; not shown) and vacuoles, respectively. *C*, comparative initial uptake rates of ^{3}H-radiolabeled hypoxanthine in FcyB mutant alleles and a wt control are shown. 100% is the transport rate in the wt (FcyB). *D*, Western blot analysis of total proteins from FcyB-GFP mutants detected with anti-GFP antibody is shown. Antibody against actin was used as an internal marker for equal loading.

1). Given the different substrate specificities of NCS1 members, this suggests that some other residues might also be critical for substrate binding, a prediction supported in this work (see later).

To test the functional role of the residues discussed above, as well as residues differentially conserved in NCS1 members with different specificity profiles or residues positioned close to the proposed binding site, we constructed a series of relevant mutations and analyzed functionally the corresponding mutants. The 19 mutations made were: N81A, N81S, S85A, V83N, W159A, N163Q, N163L, T191A, E206A, W259A, S261A, N350Q, N350D, N350A, N351A, P353A, N354Q, N354D, N354A (See supplemental Table S2). The rationale for the specific changes constructed was either to introduce Ala or highly conserved residues or replace FcyB residues with those found in other NCS1 members with different specificity.

All mutations were made in vectors carrying the FcyB orf expressed from the *uapA* promoter (see "Experimental Procedures"). This was so because the endogenous *fcyB* promoter is very weakly expressed under all conditions tested (13). The *uapA* gene encodes a very well studied uric acid-xanthine transporter (for reviews, see Refs. 2 and 12), and thus we used its promoter, which drives low but significant transcription. Furthermore, the *uapA* promoter can be totally repressed in the presence of ammonium ions or glutamine and can be induced in the presence of uric acid or the gratuitous induced 2-thioxanthine (54). In all constructs *fcyB* transcription is terminated by the 3′-flanking region of *uapA*. In one set of constructs, the FcyB orf was fused in-frame with the *gfp* orf. All plasmids were introduced in a strain lacking all endogenous purine transporters ("Experimental Procedures").

Phenotypic Analysis of FcyB Mutants—We analyzed all selected transformants on different purines as sole nitrogen sources together with positive and negative isogenic control strains. A summary of this analysis of transformants expressing single-copy FcyB plasmids is shown in Fig. 4*A*. The positive control strain expressing wild-type FcyB from the *uapA* promoter can grow on adenine and hypoxanthine as sole nitrogen sources and is sensitive to 5-FC. The negative control strain lacking FcyB cannot grow in any purine and is resistant to 5-FC. Based on our previous experience with *A. nidulans* transporters, any mutation reducing steady state rates of purine uptake to <50% that of the wild-type rate is clearly reflected in relevant growth tests. Transport reductions to levels >50% do not lead to distinguishable growth phenotypes. As expected, all strains showed normal growth on nitrogen sources other than purines (*e.g.* urea). None among the FcyB alleles conferred a capacity for growth on other purines, such as uric acid or xanthine, which are not physiological substrates for the wild-type FcyB (not shown). Within the limits of growth testing on hypoxanthine or adenine and sensitivity to 5-FC, FcyB mutants could be classified into apparent wild-type-like (E206A), total loss-of function (N81A, W159A, N163L, W259A, N350Q, P353A, N354D), or partial loss-of function (V83N, S261A) or altered specificity

showing differential capacities to grow on adenine, hypoxanthine, or 5-FC (T191A, N163Q, N350A, N350D, N351A, N354A, N354Q). In particular, mutants T191A, N351A, N354A, and N354Q grow better on adenine than on hypoxanthine, but in addition, T191A has wild-type like 5-FC sensitivity, whereas the other three mutants are significantly resistant to this toxic analog. In contrast, N163Q and N350A grow better on hypoxanthine than on adenine, but in addition, N163Q is resistant to 5-FC, whereas N350A has wild-type-like 5-FC sensitivity. N350D does not grow on hypoxanthine and adenine but is 5-FC-sensitive. The conclusions from this growth test are: (i) Asn-351 and Asn-354 are very important for hypoxanthine and 5-FC (and probably cytosine) transport but less for adenine, (ii) Asn-163 is more important for 5-FC but less critical for adenine transport and even less for hypoxanthine transport, (iii) Asn-350 is more critical for the transport of adenine and less for hypoxanthine 5-FC, and (iv) T191 seems critical solely for hypoxanthine transport.

Apparent Purine Transport Rates in FcyB Mutants—We performed comparative radiolabeled hypoxanthine uptake measurements in the strains shown in Fig. 4*A*. Our results (Fig. 4*C*) were in line with growth tests. All mutants characterized as loss-of-function had no or extremely low ($V < 6\%$) apparent uptake capacity for hypoxanthine. Partial loss-of-function mutations had 33–53% apparent uptake capacity, and E206A showed 150% transport capacity compared with wild type. Specificity mutants had low rates for hypoxanthine transport (2–15% that of the wild-type) except N350A (67%). These results showed that most amino acid residues tested, except Glu-206 and to a certain degree Val-83 and Ser-261, are critical for FcyB transport activity and substrate specificity.

Expression Levels and Cytoplasmic Localization of Mutant Versions of FcyB—Reduced apparent *V* values could imply FcyB problematic trafficking, high turnover, or *bona fide* reduction in transport activity. To distinguish among these possibilities, we reconstructed relevant FcyB alleles tagged with GFP and performed Western blots and epifluorescence microscopic analyses.

Western blot analysis of total proteins isolated by the mutants probed with anti-GFP showed that the FcyB protein steady state levels are either similar or increased (up to 6-fold) compared with the wild type (Fig. 4*D*). Increased protein steady state levels are in principle due to either increased intrinsic stability, often associated with reduced transport function, or due to reduced vacuolar turnover due to ER retention.

Epifluorescence microscopic analysis of the same mutants confirmed that the FcyB-GFP protein was expressed in all mutants and further revealed that in several mutants (N81A, S85A, N163Q, N163L, T191A, N350D, N351A, N354Q, N354D, N354A) FcyB-GFP had increased ER retention relevant to the wild-type FcyB-GFP protein (Fig. 4*B*). In fungi, the ER membrane appears mostly as very characteristic perinuclear rings, as verified by Hoechst 33242 or DAPI staining, or by fluorescent labeling of an ER resident chaperone (55–57). We have previously shown that transporters with problematic trafficking are mostly retained in these ER perinuclear rings (11, 40). We also verified the identity of the FcyB-GFP-labeled ER perinuclear rings in a relative mutant (N81A), by nuclei staining, and by examining the relative localization of these rings with histone H1 labeled with mRFP (supplemental Fig. S3). Noticeably, in some mutants (*e.g.* N81A) the FcyB-GFP signal intensity does not correspond to the protein steady state levels detected by anti-GFP (see Fig. 4*D*). This discrepancy between higher GFP signals in the cells and low level detection by Western analysis is not uncommon and is probably due to partial misfolding of proteins that might differentially affect protein turnover and GFP visualization. Also, noticeable is the observation that in mutants with more prominent ER retention the protein levels of FcyB-GFP are often higher than in wild type, probably due to reduced vacuolar turnover.

TABLE 1
Kinetic and specificity profile of mutant versions of FcyB

$K_{m/i}$ values (μM) were determined as described under "Experimental Procedures." >500 or >1000 stand for inhibition values close to 10–20% at 0.5 and 1 mM, respectively. Results are averages of at least three independent experiments in triplicate for each concentration point. S.D. was <20%.

	Hypoxanthine	Adenine	Guanine	Cytosine
WT	11	7	17	20
V83N	16	2	7	18
S85A	78	26	16	45
N163Q	47	2	>500	73
T191A	9	11	4	3
E206A	6	7	10	14
S261A	4	6	50	17
N351A	3	1	4	16
N350D	5	8	31	6
N350A	6	>1000	25	5
N354D	3	1	>500	4

Mutants related to residues Trp-159, Trp-259, and Pro-353 show a subcellular localization picture similar to wild type (no significant ER-retention), so that their lack of function should be directly associated to lack of transport activity. In mutants showing problematic FcyB trafficking, such as those concerning polar residues Asn-81, Ser-85, Asn-163, T191, Asn-350, Asn-351, and Asn-354, we cannot rigorously conclude whether the relevant residues are critical for transport activity *per se* or whether they affect transport activity indirectly due to partial misfolding. However, the fact that most of these mutants conserve minimal activity allowed us to perform a kinetic analysis and show that they are indeed critical for substrate binding (see below).

Specificity Profile of FcyB Mutants—We performed direct radiolabeled hypoxanthine uptake competition assays to define the binding constants ($K_{m/i}$s) of FcyB for its physiological substrates in the relevant mutants (for details see "Experimental Procedures"). We could only perform transporter kinetics in mutants that preserve a measurable uptake rate of hypoxanthine. These were S85A, V83N, N163Q, T191A, E206A, S261A, N350D, N350A, N351A, and N354D. Given that $K_{m/i}$ values do not depend on the number of transporter molecules expressed in the plasma membrane, for mutants showing very low hypoxanthine uptake (< 6%), such as N350D, N351A, and N354D, we used multicopy transformants for performing the kinetic analysis. Table 1 summarizes the results obtained. The mutants analyzed could be classified to those little affecting substrate binding (V83N, T191A, E206A, S261A, N350D) and those modifying significantly and, in most cases, differentially the binding of various substrates (N163Q, N350A, N351A, N354D). Among the latter, N163Q leads to a 4-fold reduction in

the binding of hypoxanthine or cytosine, >30-fold reduction in guanine binding, and a 3.5-fold increase in adenine binding. N350A conserves binding affinities for hypoxanthine, guanine, and cytosine close to those of the wild-type (moderately increased binding for hypoxanthine and cytosine) but exhibits a dramatic loss of adenine binding ($K_i > 1000\ \mu M$). N351A has a general tendency to bind with higher affinity (4–7-fold) all purines, but not cytosine. Finally, N354D has a 4-fold increased capacity for hypoxanthine, adenine, and cytosine binding but a dramatic loss of guanine binding ($K_i > 500\ \mu M$). Noticeably, the dramatic differential effect of mutation N350A on the ability of FcyB to bind adenine *versus* hypoxanthine or cytosine binding was nicely reflected in growth tests showing that N350A grows better on hypoxanthine than on adenine and is sensitive to 5-FC (see Fig. 4*A*). In summary, kinetic analysis of mutants showed that residues Asn-163, Asn-350, and Asn-354 are critical for substrate specificity, whereas Asn-163 and Asn-350 are mostly critical for substrate binding affinities.

DISCUSSION

Evidence from structural studies and molecular simulations have strongly supported the proposal that the transporters of the 5HIR superfamily function by an alternating access mechanism in which substrate binding triggers a conformational change from an outward-facing open conformation through an occluded structure to the an inward-facing open state of the protein (32–34, 36, 39). However, many aspects of this mechanism, as for example the exact steps along the substrate and ion translocation pathway or how gating operates in each case, remain to be investigated. Our current work did not intend to approach the alternating mechanism of transport by members of the 5HIR superfamily. It rather focused on the identification of specific residues that determine the function, transport kinetics, and substrate specificity of a eukaryotic member of the NCS1 family.

The first part of our work presents a theoretical structural model of the FcyB purine-cytosine transporter that reveals a number of important aspects concerning how this transporter might bind and transport its substrates. To validate the theoretical conclusions, we proceeded in a systematic mutational analysis of putatively critical residues. Our experimental results fully support the involvement of specific residues in TMS1, TMS3, TMS6, and TMS8 in substrate binding and/or transport. In particular, residues Ser-85, Trp-159, Asn-163, Trp-259, Asn-350, Asn-351, Pro-353, and Asn-354 were shown to be irreplaceable for FcyB-mediated transport. Among these residues, Ser-85, Asn-163, Asn-350, Asn-351, and Asn-354 seem critical for determining the substrate binding affinity and/or specificity of FcyB (see Fig. 4 and Table 1). Among the irreplaceable amino acids, Asn-163 and Asn-351 might also affect FcyB stability or/and turnover as the GFP-tagged versions of these alleles are significantly blocked in the ER compared with the wild-type protein. The other residues analyzed, Asn-81, Val-83, Ser-261, Thr-191, and Glu-206, seem to have a less critical role on protein turnover or FcyB transport activity. Only mutation T191A moderately affects the affinity and substrate specificity of FcyB. Noticeably, E206A, a residue within TMS5 that has been reported to function as a putative inward-facing gate, leads to a reduction in FcyB turnover and an increase in apparent transport capacity (see Fig. 4).

Among the eight residues essential for FcyB function and specificity, Trp-159, Asn-163, Trp-259, Asn-350, and Asn-354 correspond to residues shown to be directly involved in substrate binding by the Mhp1 transporter (Trp-117, Gln-121, Trp-220, Asn-314, and Asn-318). Ser-85 is similarly, but not identically positioned, with Gln-42 in Mhp1, which is also involved in substrate binding. The rest two essential FcyB residues, Asn-351 and Pro-353, are within hydrogen bonding distance with residues proposed to be involved in direct substrate binding such that they may hold the local architecture of the binding site in a position to interact with substrates. Thus, FcyB and Mhp1, despite their important specificity difference and overall low amino acid sequence identity, share very similar residues to build their substrate binding sites; four residues are identical (Trp-159, Trp-259, Asn-350, and Asn-354, numbering of FcyB), one is highly conserved (Asn-163 of FcyB replaced by Gln-121 in Mhp1), and three are not conserved (Ser-85, Asn-351, and Pro-353 in FcyB *versus* Gln-42, Pro-315, and Ala-317 in Mhp1). In fact, the four absolutely conserved residues between FcyB and Mhp1 are also highly conserved in all NCS1 members, whereas the other four residues are differentially conserved among different homologues (see Fig. 1). In particular, Asn-163 is conserved in nearly all purine-cytosine Fcy-like NCS1 members, replaced by a Glu residue in a plant adenine-guanine-uracil transporter (AtNcs1), by a Gln in homologues specific for uracil (Fur4p/FurD) or allantoin (Dal4p/FurA), and by a Leu in a uridine-specific transporter (Fui1p). Asn-351 and Pro-353 are conserved in microbial NCS1 members specific for purine-cytosine (Fcy-like proteins) but are replaced by Ile and Ala in the plant adenine-guanine-uracil transporter (AtNcs1) and the uracil- or allantoin-specific transporters (Fur4p, FurD, FurA, and Dal4p) or by Leu and Gly in a uridine-specific homologue (Fui1p). Interestingly, Ser-85, a major amino acid in FcyB function, is not a conserved residue in the NCS1 family.

None of the single mutations constructed and analyzed in this work, including N163L, N163Q, or P353A, which introduce residues present in uracil, allantoin, hydantoin, or uridine transporters, conferred to FcyB the ability to bind or/and transport substrates other than adenine, guanine, hypoxanthine, and cytosine (results not shown). In fact, mutations N163L, N163Q, or P353A led to loss or highly reduced transport capacity of FcyB. This observation strongly suggests that substrate specificity has a more complex molecular basis and might not even be solely determined by the architecture of the binding site but also by elements acting as gates or selectivity filters or by elements contributing to protein stability. We have arrived at a similar conclusion with respect to the role of interdomain synergy in determining the specificity of another group of purine transporters, the nucleobase-ascorbate transporter (NAT/NCS2) family, which was extensively studied in our laboratory (40–42).

A genetic analysis of Fcy2p, a true orthologue of FcyB in *S. cerevisiae*, supports results presented in this work. Genetically selected and subsequent site-directed mutations have strongly suggested a major role of residues Asn-374, Pro-376, and Asn-377, equivalent to Asn-351, Pro-353, and Asn-354 in

FcyB, in substrate binding (18–19). Noticeably, the effects of mutations in Asn-374 and Asn-377 were partially due to a shift of the pK_a of an ionizable amino acid residue of the unliganded transporter (18). Interestingly, mutation S272L in TMS6, isolated as an allele nonspecific, second-site, suppressor of loss-of-function mutations T213I, N374I, or N377G, partially restored the binding of hypoxanthine and cytosine (19).

Based on the above comparative observations, the docking results with FcyB, and the mutational analysis presented herein, we propose that residues corresponding to Trp-159, Trp-259, Asn-350, Pro-353, and Asn-354 in FcyB are major elements of the substrate binding site in all NCS1 members, whereas residues corresponding to Ser-85, Asn-163, and Asn-351 are mostly specificity determinants. We propose that residues Ser-85, Asn-163, and Asn-354 make direct H-bonds with substrates and Trp-159 and Trp-259 stabilize binding through π-π-stacking interactions with the purine or pyrimidine ring, whereas residues Asn-350, Asn-351, and Pro-353 have an indirect role in substrate binding through local interactions between themselves and the residues binding substrates. The critical role of residues of the four Asn residues, Asn-163, Asn-350, Asn-351, and Asn-354, in FcyB function and specificity is strongly supported by both growth phenotypes and kinetic profiles of the corresponding mutants (Fig. 4*A* and Table 1). For example, FcyB-N350A binds similarly to wild-type FcyB hypoxanthine, guanine, and cytosine but has lost the capacity for adenine binding. FcyB-N350D has increased binding affinity specifically for hypoxanthine and 5-FC, but only the latter is transported efficiently. N354D or N163Q have specifically lost the ability to bind guanine. Finally, N351A, N354A, and N354Q transport adenine much more efficiently than hypoxanthine and 5-FC, as deduced from the growth tests shown in Fig. 4*A* (a similar growth phenotype is also exhibited by N351I; results not shown).

Our work is the first systematic functional analysis of a eukaryotic member of the NCS1 family that, moreover, is combined with theoretical approaches concerning the three-dimensional transporter structure. Given the privilege of the several Mhp1 crystal structures available corresponding to different conformations achieved during transport catalysis, we are now in a position to perform a second round of rational mutagenesis combined with unique genetic screens available in *A. nidulans* to understand in more detail not only how FcyB works and selects its substrates but also how substrate specificity has evolved within the NCS1 family.

Acknowledgment—All molecular dynamic simulations were run on Cy-tera high performance computing (HPC) facility.

REFERENCES

1. de Koning, H., and Diallinas, G. (2000) Nucleobase transporters (review). *Mol. Membr. Biol.* **17,** 75–94
2. Gournas, C., Papageorgiou, I., and Diallinas, G. (2008) The nucleobase-ascorbate transporter (NAT) family. Genomics, evolution, structure-function relationships, and physiological role. *Mol. Biosyst.* **4,** 404–416
3. de Koning, H. P., Bridges, D. J., and Burchmore, R. J. (2005) Purine and pyrimidine transport in pathogenic protozoa. From biology to therapy. *FEMS Microbiol. Rev.* **29,** 987–1020
4. Schultes, N. P., Brutnell, T. P., Allen, A., Dellaporta, S. L., Nelson, T., and Chen, J. (1996) Leaf permease1 gene of maize is required for chloroplast development. *Plant Cell* **8,** 463–475
5. Mourad, G. S., Snook, B. M., Prabhakar, J. T., Mansfield, T. A., and Schultes, N. P. (2006) A fluoroorotic acid-resistant mutant of *Arabidopsis* defective in the uptake of uracil. *J. Exp. Bot.* **57,** 3563–3573
6. Zrenner, R., Stitt, M., Sonnewald, U., and Boldt, R. (2006) Pyrimidine and purine biosynthesis and degradation in plants. *Annu. Rev. Plant Biol.* **57,** 805–836
7. Kraupp, M., and Marz, R. (1995) Membrane transport of nucleobases. Interaction with inhibitors. *Gen. Pharmacol.* **26,** 1185–1190
8. Köse, M., and Schiedel, A. C. (2009) Nucleoside/nucleobase transporters. Drug targets of the future? *Future Med. Chem.* **1,** 303–326
9. Barrett, M. P., and Gilbert, I. H. (2006) Targeting of toxic compounds to the trypanosome's interior. *Adv. Parasitol.* **63,** 125–183
10. Pfaller, M. A. (2012) Antifungal drug resistance. Mechanisms, epidemiology, and consequences for treatment. *Am. J. Med.* **125,** S3–S13
11. Pantazopoulou, A., and Diallinas, G. (2007) Fungal nucleobase transporters. *FEMS Microbiol. Rev.* **31,** 657–675
12. Diallinas G., and Gournas C. (2008) Structure-function relationships in the nucleobase-ascorbate transporter (NAT) family. Lessons from model microbial genetic systems. *Channels* **2,** 363–372
13. Vlanti, A., and Diallinas G. (2008) The *Aspergillus nidulans* FcyB cytosine-purine scavenger is highly expressed during germination and in reproductive compartments and is down-regulated by endocytosis. *Mol. Microbiol.* **68,** 959–977
14. Hamari, Z., Amillis, S., Drevet, C., Apostolaki, A., Vágvölgyi, C., Diallinas, G., and Scazzocchio, C. (2009) Convergent evolution and orphan genes in the Fur4p-like family and characterization of a general nucleoside transporter in *Aspergillus nidulans*. *Mol. Microbiol.* **73,** 43–57
15. Mourad, G. S., Tippmann-Crosby, J., Hunt, K. A., Gicheru, Y., Bade, K., Mansfield, T. A., and Schultes, N. P. (2012) Genetic and molecular characterization reveals a unique nucleobase cation symporter 1 in *Arabidopsis*. *FEBS Lett.* **586,** 1370–1378
16. Weber, E., Rodriguez, C., Chevallier, M. R., and Jund, R. (1990) The purine-cytosine permease gene of *Saccharomyces cerevisiae*. Primary structure and deduced protein sequence of the FCY2 gene product. *Mol. Microbiol.* **4,** 585–596
17. Goudela, S., Tsilivi, H., and Diallinas, G. (2006) Comparative kinetic analysis of AzgA and Fcy21p, prototypes of the two major fungal hypoxanthine-adenine-guanine transporter families. *Mol. Membr. Biol.* **23,** 291–303
18. Ferreira, T., Brèthes, D., Pinson, B., Napias, C., and Chevallier, J. (1997) Functional analysis of mutated purine-cytosine permease from *Saccharomyces cerevisiae*. A possible role of the hydrophilic segment 371–377 in the active carrier conformation. *J. Biol. Chem.* **272,** 9697–9702
19. Ferreira, T., Chevallier, J., Paumard, P., Napias, C., and Brèthes, D. (1999) Screening of an intragenic second-site suppressor of purine-cytosine permease from *Saccharomyces cerevisiae*. Possible role of Ser-272 in the base translocation process. *Eur. J. Biochem.* **260,** 22–30
20. Ferreira, T., Napias, C., Chevallier, J., and Brèthes, D. (1999) Evidence for a dynamic role for proline 376 in the purine-cytosine permease of *Saccharomyces cerevisiae*. *Eur. J. Biochem.* **263,** 57–64
21. Suzuki, S., and Henderson, P. J. (2006) The hydantoin transport protein from *Microbacterium liquefaciens*. *J. Bacteriol.* **188,** 3329–3336
22. Weyand, S., Shimamura, T., Yajima, S., Suzuki, S., Mirza, O., Krusong, K., Carpenter, E. P., Rutherford, N. G., Hadden, J. M., O'Reilly, J., Ma, P., Saidijam, M., Patching, S. G., Hope, R. J., Norbertczak, H. T., Roach, P. C., Iwata, S., Henderson, P. J., and Cameron, A. D. (2008) Structure and molecular mechanism of a nucleobase-cation-symport-1 family transporter. *Science* **322,** 709–713
23. Yamashita, A., Singh, S. K., Kawate, T., Jin, Y., and Gouaux, E. (2005) Crystal structure of a bacterial homologue of Na^+/Cl^--dependent neurotransmitter transporters. *Nature* **437,** 215–223
24. Faham, S., Watanabe, A., Besserer, G. M., Cascio, D., Specht, A., Hirayama, B. A., Wright, E. M., and Abramson, J. (2008) The crystal structure of a sodium galactose transporter reveals mechanistic insights into Na^+/sugar symport. *Science* **321,** 810–814

25. Ressl, S., Terwisscha van Scheltinga, A. C., Vonrhein, C., Ott, V., and Ziegler, C. (2009) Molecular basis of transport and regulation in the Na^+/betaine symporter BetP. *Nature* **458,** 47–52
26. Fang, Y., Jayaram, H., Shane, T., Kolmakova-Partensky, L., Wu, F., Williams, C., Xiong, Y., and Miller, C. (2009) Structure of a prokaryotic virtual proton pump at 3.2 Å resolution. *Nature* **460,** 1040–1043
27. Shaffer, P. L., Goehring, A., Shankaranarayanan, A., Gouaux, E. (2009) Structure and mechanism of a Na^+-independent amino acid transporter. *Science* **325,** 1010–1014
28. Chen, N. H., Reith, M. E., and Quick, M. W. (2004) Synaptic uptake and beyond. The sodium- and chloride-dependent neurotransmitter transporter family SLC6. *Pflugers Arch.* **447,** 519–531
29. Wright, E. M., Hirayama, B. A., and Loo, D. F. (2007) Active sugar transport in health and disease. *J. Intern. Med.* **261,** 32–43
30. Yanagida, O., Kanai, Y., Chairoungdua, A., Kim, D. K., Segawa, H., Nii, T., Cha, S. H., Matsuo, H., Fukushima, J., Fukasawa, Y., Tani, Y., Taketani, Y., Uchino, H., Kim, J. Y., Inatomi, J., Okayasu, I., Miyamoto, K., Takeda, E., Goya, T., and Endou, H. (2001) Human L-type amino acid transporter 1 (LAT1). Characterization of function and expression in tumor cell lines. *Biochim. Biophys. Acta* **1514,** 291–302
31. Harada, N., Nagasaki, A., Hata, H., Matsuzaki, H., Matsuno, F., and Mitsuya, H. (2000) Down-regulation of CD98 in melphalan-resistant myeloma cells with reduced drug uptake. *Acta Haematol.* **103,** 144–151
32. Abramson, J., and Wright, E. M. (2009) Structure and function of Na^+ symporters with inverted repeats. *Curr. Opin. Struct. Biol.* **19,** 425–432
33. Krishnamurthy, H., Piscitelli, C. L., and Gouaux, E. (2009) Unlocking the molecular secrets of sodium-coupled transporters. *Nature* **459,** 347–355
34. Shimamura, T., Weyand, S., Beckstein, O., Rutherford, N. G., Hadden, J. M., Sharples, D., Sansom, M. S., Iwata, S., Henderson, P. J., and Cameron, A. D. (2010) Molecular basis of alternating access membrane transport by the sodium-hydantoin transporter Mhp1. *Science* **328,** 470–473
35. Singh, S. K., Piscitelli, C. L., Yamashita, A., and Gouaux, E. (2008) A competitive inhibitor traps LeuT in an open-to-out conformation. *Science* **322,** 1655–1661
36. Krishnamurthy, H., and Gouaux, E. (2012) X-ray structures of LeuT in substrate-free outward-open and apo inward-open states. *Nature* **481,** 469–474
37. Gao, X., Lu, F., Zhou, L., Dang, S., Sun, L., Li, X., Wang, J., and Shi, Y. (2009) Structure and mechanism of an amino acid antiporter. *Science* **324,** 1565–1568
38. Weyand, S., Shimamura, T., Beckstein, O., Sansom, M. S., Iwata, S., Henderson, P. J., and Cameron, A. D. (2011) The alternating access mechanism of transport as observed in the sodium-hydantoin transporter Mhp1. *J. Synchrotron. Radiat.* **18,** 20–23
39. Adelman, J. L., Dale, A. L., Zwier, M. C., Bhatt, D., Chong, L. T., Zuckerman, D. M., and Grabe, M. (2011) Simulations of the alternating access mechanism of the sodium symporter Mhp1. *Biophys. J.* **101,** 2399–2407
40. Papageorgiou, I., Gournas, C., Vlanti, A., Amillis, S., Pantazopoulou, A., and Diallinas, G. (2008) Specific interdomain synergy in the UapA transporter determines its unique specificity for uric acid among NAT carriers. *J. Mol. Biol.* **382,** 1121–1135
41. Kosti, V., Papageorgiou, I., and Diallinas, G. (2010) Dynamic elements at both cytoplasmically and extracellularly facing sides of the UapA transporter selectively control the accessibility of substrates to their translocation pathway. *J. Mol. Biol.* **397,** 1132–1143
42. Amillis, S., Kosti, V., Pantazopoulou, A., Mikros, E., and Diallinas, G. (2011) Mutational analysis and modeling reveal functionally critical residues in transmembrane segments 1 and 3 of the UapA transporter. *J. Mol. Biol.* **411,** 567–580
43. Sali, A., and Blundell, T. L. (1993) Comparative protein modeling by satisfaction of spatial restraints. *J. Mol. Biol.* **234,** 779–815
44. Jorgensen, W. L., Maxwell, D. S., and Tirado-Rives, J. (1996) Development and testing of the OPLS all-atom force field on conformational energetics and properties of organic liquids. *J. Am. Chem. Soc.* **118,** 11225–11236
45. Bowers, K., Chow, E., Xu, H., O. Dror, R., Eastwood, M. P., Gregersen, B. A., Klepeis, J. L., Kolossvary, I., Moraes, M. A., Sacerdoti, F. D., Salmon, J. K., Shan, Y., and Shaw, D. E. (2006) *Proceedings of the ACM/IEEE Conference on Supercomputing (SC06)*, Tampa, Florida, November 11–17, 2006
46. Lomize, M. A., Lomize, A. L., Pogozheva, I. D., and Mosberg, H. I. (2006) OPM. Orientations of proteins in membranes database. *Bioinformatics* **22,** 623–625
47. Sherman, W., Day, T., Jacobson, M. P., Friesner, R. A., Farid, R. (2006) Novel procedure for modeling ligand/receptor induced fit effects. *J. Med. Chem.* **49,** 534–553
48. Koukaki, M., Giannoutsou, E., Karagouni, A., and Diallinas, G. (2003) A novel improved method for *Aspergillus nidulans* transformation. *J. Microbiol. Methods.* **55,** 687–695
49. Edgerton-Morgan, H., and Oakley, B. R. (2012) γ-Tubulin plays a key role in inactivating APC/C^{Cdh1} at the G_1-S boundary. *J. Cell Biol.* **198,** 785–791
50. Diallinas, G., Gorfinkiel, L., Arst, H. N. Jr., Cecchetto, G., and Scazzocchio, C. (1995) Genetic and molecular characterization of a gene encoding a wide specificity purine permease of *Aspergillus nidulans* reveals a novel family of transporters conserved in prokaryotes and eukaryotes. *J. Biol. Chem.* **270,** 8610–8622
51. Sambrook, J., Fritsch, E. F., and Maniatis, T. (1989) *Molecular Cloning: A Laboratory Manual*, 2nd Ed., Cold Spring Harbor Laboratory, Cold Spring Harbor, NY
52. Gournas, C., Amillis, S., Vlanti, A., and Diallinas, G. (2010) Transport-dependent endocytosis and turnover of a uric acid-xanthine permease. *Mol. Microbiol.* **75,** 246–260
53. Cecchetto, G., Amillis, S., Diallinas, G., Scazzocchio, C., and Drevet, C. (2004) The AzgA purine transporter of *Aspergillus nidulans*. Characterization of a protein belonging to a new phylogenetic cluster. *J. Biol. Chem.* **279,** 3132–3141
54. Gorfinkiel, L., Diallinas, G., and Scazzocchio, C. (1993) Sequence and regulation of the uapA gene encoding a uric acid-xanthine permease in the fungus *Aspergillus nidulans*. *J. Biol. Chem.* **268,** 23376–23381
55. Amillis, S., Cecchetto, G., Sophianopoulou, V., Koukaki, M., Scazzocchio, C., Diallinas, G. (2004) Transcription of purine transporter genes is activated during the isotropic growth phase of *Aspergillus nidulans* conidia. *Mol. Microbiol.* **52,** 205–216
56. Vlanti, A., Amillis, S., Koukaki, M., Diallinas, G. (2006) A novel-type substrate selectivity filter and ER exit determinants in the UapA purine transporter. *J. Mol. Biol.* **357,** 808–819
57. Erpapazoglou, Z., Kafasla, P., and Sophianopoulou, V. (2006) The product of the SHR3 orthologue of *Aspergillus nidulans* has a restricted range of amino acid transporter targets. *Fungal Genet. Biol.* **43,** 222–233